ACS APPLIED ELECTRONIC MATERIALS

Article

Cite This: ACS Appl. Electron. Mater. 2019, 1, 752−763

pubs.acs.org/acsaelm

Electrochemical Erasing Using a Polymer Lithography Editor for the Fabrication of Photoactive Devices

Nathalie Becerra-Mora,[†] Annie Y. Vargas-Lizarazo,[†] Connor Orrison,[‡] Monica Barron,[§] Rajesh P. Balaraman,[†] and Punit Kohli*[,†]

[†]Department of Chemistry and Biochemistry, Southern Illinois University, Carbondale, Illinois 62901, United States

[‡]Old Dominion University, Norfolk, Virginia 23529, United States

[§]Department of Chemistry and Chemical Biology, Indiana University-Purdue University at Indianapolis, Indianapolis, Indiana 46202, United States

Supporting Information

ABSTRACT: Electrochemical erasing of conductive coatings at microscale for the fabrication of functional devices on flexible and hard surfaces is demonstrated. The nanoporous pyramidal-shaped nano- and microscale polyacrylamide hydrogel PLE probes allowed delivery of electrochemical etchants to the surface, providing on-demand maskless patterning at microscale. Highly efficient erasing (silver and copper metals erasing efficiency ≈ 100%), areal erasing rate ≈ 80 $\mu m^2/s$, and pressure dependent spatial erasing feature dimensions between 3 μm to many tens of microns on metal surfaces allowed for the fabrication of microelectrodes of various geometries. Overall, PLE-based microscale erasing allowed for rapid and accessible fabrication of organic electron−hole carrier pair-based microphotodetector, as well as the assembly of LED on flexible and rigid ITO substrates.

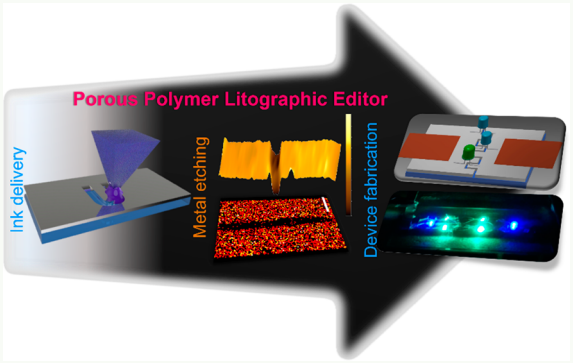

KEYWORDS: *lithographic editor, electrochemical etching, hydrogel, device fabrication, microphoto-detector*

INTRODUCTION

Dip-pen nanolithography (DPN),[1−4] polymer-pen lithography (PPL),[5−7] microcontact printing (μCP),[8] and nanofountain pen (NFP)[9−11] have been demonstrated for selective delivery and patterning of a large number of molecules[2] on a variety of surfaces.[12] A plethora of studies[3] are published for improving the delivery and the patterning of a large variety of molecules,[13−16] the spatial resolution,[7] and throughput rate.[17] The patterned surfaces and devices fabricated using these techniques possess a wide range of potential applications in bioengineering,[18] medical diagnostics,[19,20] and the electronics industry,[21,22] and the number of studies is expected to grow further.[23]

The tip probe-based deposition using DPN, PPL, and NFP are well-suited for achieving ultrahigh patterning resolution below 100 nm. DPN is capable of achieving spatial resolution patterning as low as 15 nm over large areas.[24] For large-scale patterning, a reservoir of molecular ink allows for a continuous supply of ink. For example, ink reservoirs containing NFP can allow patterning at large scale without a need to redeposit ink in the probes.[25] For example, use of a cantilever coated with PDMS yielded nanostructures within a range of 60−470 nm.[26] The reservoirs have also allowed for storage of a large amount of ink molecules and particles for deposition.[17] Additionally, control over the patterning area by changing the pen-substrate contacting area was also demonstrated using soft PDMS probes.[27] Analogously, hydrogel matrixes can be loaded with a large amount of aqueous-ink molecules with several orders higher concentration as compared to nonporous probes,[28] allowing for the delivery and deposition of molecules over large areas.[29,30]

In general, probe-based erasing and patterning requires formation of a meniscus between the probe and the substrate. This is usually achieved when the probe is brought near a desired surface, resulting in the transfer of molecules from the probe to the surface. In the case of PPL, the transfer of ink can occur through the meniscus at the substrate-probe interface and through direct contact between the tip and substrate as well. This molecule transport mechanism is comparable to the deposition mechanism involved in μCP. The rate of molecular transport from the probe to the substrate is dependent on the physical and chemical characteristics of the ink,[31] substrate, tip material properties,[32] and environmental conditions, such as temperature and relative humidity.[33] Ink-tip and ink-substrate interactions are key processes that also affect the size of the patterned features in the probe-based patterning. Although the

Received: February 18, 2019
Accepted: April 22, 2019
Published: April 22, 2019

DOI: 10.1021/acsaelm.9b00099
ACS Appl. Electron. Mater. 2019, 1, 752−763

Scheme 1. Flow Chart for the Si Master Fabrication through Photolithography and HF Anisotropic Etching[a]

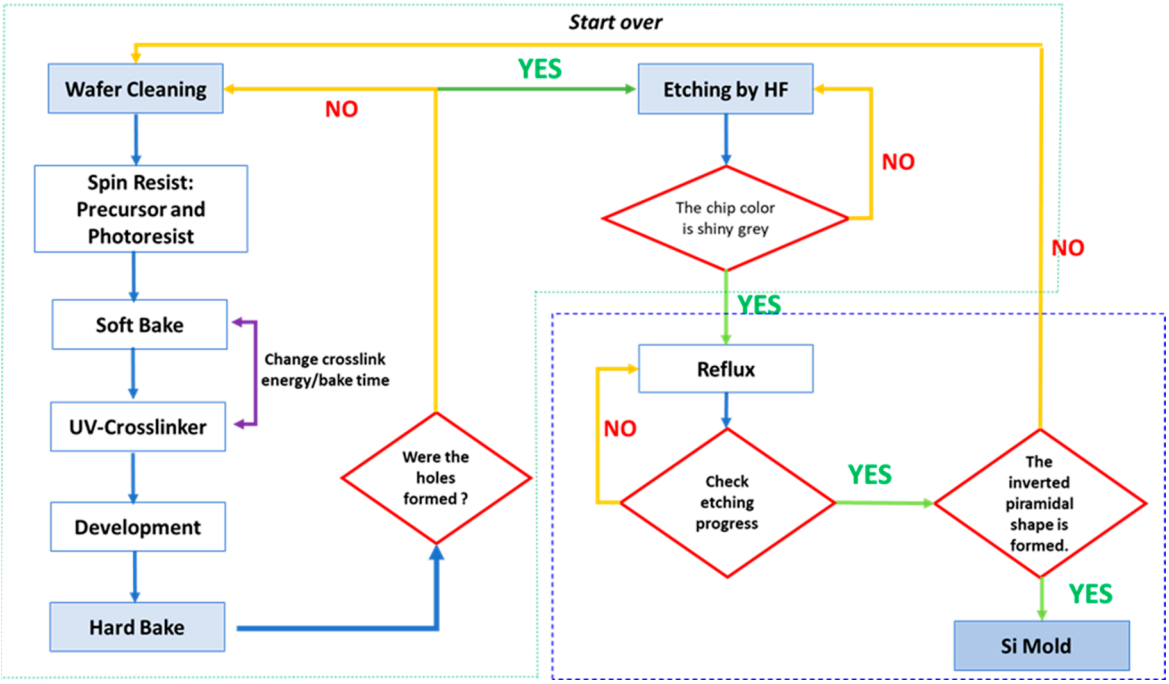

[a]Figure S1 shows the optical micrographs of the wafer and the pores at various stages.

concentration difference-based passive diffusion and/or through fluid dynamics[34] are dominantly used for molecular transport for the surface patterning, a much higher patterning rate (~2−3 orders of magnitude larger than those observed in the passive transport probe delivery systems) can accomplish the application of an external electrical potential stimulus between the probe and substrate.[10,35]

Although the molecular deposition using probe-based techniques is broadly investigated, the studies describing the selective removal of molecules from surfaces are limited in the literature. For example, nanoshaving,[36] nanografting,[37] and electrochemical removal using a conductive atomic force microscope (AFM) tip[38] are demonstrated for molecular removal and erasing. Because of the serial probe movements at the nanometer scale during erasing, these techniques can be expensive and time-consuming.[39] For example, in the case of nanoshaving and nanodrafting, the mechanical erasing requires intimate probe-surface contact that may damage and/or induce defects in probe tips and substrates. Recently, an error rectifying method using a polymer lithography editor (PLE) was introduced, where a soft probe composed of agarose hydrogel allowed for molecular erasing and writing mediated through a meniscus formed between the probe and substrate.[40] The rectification process "writing−erasing−rewriting" was demonstrated by "writing" ~10 μm fluorescein array dots on the glass substrate. The accuracy of erasing was demonstrated by placing the PLE eraser within 700 nm of a given registration spot; "rewriting" with fluorescein using PLE at the erased area completed the editing process. The erasing process in PLE involves two major steps. An initial step involves the solvation of the patterned molecules by solvent molecules transported from the tip or molecules that are already present on the substrate surface. This is followed by a second step, where solvated molecules diffuse into the nanoporous PLE tip matrix driven by the concentration gradient.[40] Similarly, the writing/rewriting process was accomplished by transport of the ink molecules through the meniscus at the PLE probe−substrate interface. PLE was also utilized for the fabrication of the functional photoactive microdevices in this study.

Manipulation of physical and chemical properties of the conductive and elastomeric materials has led to the development of flexible electronics devices. These devices possess a wide range of potential applications, including, but not limited to, nonlinear electronic eyeball cameras, deformable LEDs, 3D micro/nanostructures and functional devices, flexible diagnostic devices for brain surgery, and interfaces for human−computer control systems and related biointegrated devices.[41−49] The PLE-based lithography is complementary to many lithographic deposition and patterning techniques presently used in industry.

In this article, we show that polyacrylamide (PAAM) hydrogel PLE probes delivered electrochemical etchant molecules selectively to carry out reactions at the microscale level for the functional device fabrication. We demonstrate electrochemical etching of multielectrode materials (silver, copper, and indium tin oxide) for the fabrication of interdigitated electrodes on soft and hard substrates. The interdigitated electrodes were used to fabricate microphotodetectors using a deposition of an organic electron−hole pair (P3HT−bis[60]PCBM) on hard substrates. Further, the assembling of LED was accomplished using PLE-assisted microelectrodes fabricated on both hard and flexible substrates. Using PLE, this work demonstrates the fabrication of microscale functional devices in wet laboratory conditions without a need of traditional clean room lithography facilities.

Overall, due to selective spatial etching, PLE allows for the fabrication of devices on a variety of substrates, including both soft and hard materials and those that may be susceptible to multistep harsh conditions employed in traditional photolithography. Importantly, PLE provides mask-less on-demand

DOI: 10.1021/acsaelm.9b00099
ACS Appl. Electron. Mater. 2019, 1, 752−763

electrochemical etching at the microscale over large areas in ambient wet conditions. Clean-room conditions are optional for microscale patterning when utilizing PLE. Thus, the main attractive feature of the PLE is that by simple programming of a microstage allows fabrication of desired metallic, nonmetallic, and semi-conductive patterns with microscale features under ambient laboratory conditions. Thus, the use of PLE-based fabrication can be potentially useful for fast prototyping without the need of extensive instrumentation and clean room facility.

EXPERIMENTAL SECTION

Materials. MCC Primer 80/20 was purchased from Micro Chem. ME 351 (microdeposit 351 developer) and S1805 photoresist (microposit S1805 positive photoresist) were obtained from ROHM and HAAS Electronic Materials, Massachusetts. Buffered-HF was purchased from Transene Company, Inc., Danvers, MA. Pyrocathecol (Cathecol 99%) was obtained from Alfa Aesar. Ethylene diamine 99% (extra pure), ammonium persulfate 98% (extra pure), acrylamide 99%, hydrogen peroxide 30%, and sulfuric acid were purchased from Fisher Scientific. Bis-acrylamide was purchased from Amresco, and *N*,*N*,*N*′,*N*′-tetramethylenediamine 99% (extra pure, TEMED), ferric chloride, and poly(3-hexylthiophene-2,5-diyl) (P3HT, MW 85 000−100 000) were obtained from Sigma-Aldrich. Bis[60]PCBM and potassium permanganate were obtained from TCI and Mallinckrodt, respectively.

Characterization and Methods. The electronic absorption spectrum of bis[60]PCBM and P3HT in *o*-dichlorobenzene were acquired using a PerkinElmer Lambda 25 spectrometer with a slit width of 1 nm. Emission spectroscopy was performed using a PerkinElmer LS 55 spectrometer. Both the excitation and emission slit widths were 3.0 nm, and the scanning speed for the acquisition of the spectra was 50 nm/min. The photoinduced current (PIC) measurements were accomplished using a Keithley 6487 picoammeter/voltage source. A xenon arc lamp (300 W) controlled by a power supply (model no. 69907, Newport) provided photoexcitation for photoelectron-induced studies. The optical characterization of the hydrogel pen and electrochemical metal erasing was performed using a bright-field inverted Leica DMIRB microscope.

Scanning Electron Microscopy (SEM) and Energy Dispersive X-ray Spectroscopy (EDS). SEM was performed using an FEI Quanta FEG 450 SEM equipped with an EDX MaxX 50 mm^2 Oxford detector controlled using an INCA software. SEM images and EDS were acquired at an accelerating voltage of 10−20 kV. Nonconductive samples for SEM analysis were coated with a silver or gold−palladium layer (thickness ∼100−150 Å).

AFM. The AFM measurements were performed using Autoprobe Thermomicroscopes in contact mode. The microscope was controlled using ThermoMicroscopes ProScan version 1.6 Beta software. The sample was probed with a silicon nitride tip MLCT-AUMT-A with a nominal force constant given by the manufacturer of 30 pN/nm.

Fabrication of PAAM PLE Probes. *Pyramidal Silicon Master Fabrication Using Photolithography.* The fabrication of array pyramidal pores was accomplished using anisotropic etching of the Si(100) plane.[50] To guide future researchers in the fabrication of lithographic patterning, we provide a detailed flowchart and give some tips that may be helpful for the fabrication of multiple pyramidal pores (Scheme 1). In addition, with the aim to help readers, we captured a sequence of images at each key step of the methodology (Figure S1). A detailed procedure of the mold fabrication (photolithography and Si anisotropic etching) can be found in the Supporting Information.

Fabrication of Hydrogel Probes. PAAM hydrogel was chosen because its mechanical properties and porosity can be modulated by a monomer (acrylamide, *M*) to cross-linker (bis-acrylamide, *C*) ratio (R_{MC}). For example, a variation in the R_{MC} can provide PAAM with a wide range of Young's modulus, porosity, and pore size.[51] The porosity of the PAAM hydrogels enables large capacity for hydrophilic material that can be stored within the pores, and it also facilitates the transfer of solute and solvent from/to pores to/from bulk solution.

Prior to the formation of the PAAM PLE probes, the surface of the Si chips was cleaned using O_2 plasma for 120 s (power 250 W, Ar 80%, and 20% O_2). The hydrogel mixture was prepared as follows, 250 μL of acrylamide (AM, 100% w/v), 50 μL of bis-acrylamide (bAM, 2% w/v), and 25 μL of APS (initiator, 10% w/v) were vigorously mixed in a 2 mL tube. This mixture was kept in an ice bath for 2 min, and 2 μL of TEMED (catalyst) was added along the inner walls of the tube. A homogeneous distribution of the components in the solution ensured uniform cross-linking and polymerization within the matrix of the hydrogel. Then, 180 μL of this solution was added promptly to a Si chip template containing 16 pyramidal shape pores. The PAAM cross-linking process was rapid and was observed to occur within 2 min of adding the mixture into the pores. Once the PAAM hydrogel was gelled, it was peeled off from the template and stored in nanopure water at 4 °C until further use. The treatment of the pore templates was not found to be necessary for the release of the polymer probes from the templates.

Microscale Electrochemical Erasing Using PLE-Based Probes. The microphotodetectors on the PLE probe-etched interdigitated electrodes were fabricated by the deposition of an organic electron−hole active pair on the electrodes. Briefly, sputtered 100 nm thick silver or copper films with a 10 nm thick Cr adhesion layer on glass slides was used. The metal substrate was placed on a Leica DMRIB inverted microscope with a Ludl-computerized stage that controlled the *x*- and *y*-direction movements using an Oasis Blue PCI controller card. The PLE probe was attached to a *z*-axis piezoelectric stage and was brought close to the substrate at a vertical speed (v_z) of 0.1 μm/s with a step size of 150 nm. The erasing process was followed on an inverted microscope in transmission mode using microscope objectives (10× and 20× with numerical apertures of 0.25 and 0.40, respectively). The microscope was equipped with a camera Photometrics CoolSNAP Myo. Briefly, a PAAM PLE containing either a Ag etchant (KI + I_2, TFS from Transene Inc.) or Cu etchant (Fe(III), CE-200 Transene Inc.) was allowed to make contact with the metal coating using a *z*-axis piezoelectric stage. For ITO etching, an acidic solution of Fe(III) containing a PAAM single pen attached to the *z*-piezoelectric stage. The PLE probe formed a liquid meniscus between the probe and substrate delivering redox etchants to the substrate that resulted in the erasing (etching) of the metal coating. The relative humidity for all the experiments was 40 ± 10%. For copper- and silver-coated substrates, the chromium adhesion layer in-between Cu or Ag and the glass was removed by dipping the substrates in an alkaline potassium permanganate solution. After removal of the chromium etchant, the substrate was rinsed with copious amounts of water and ethanol, and then it was followed by air drying. The complete removal of metal coating was confirmed by measuring the electrical resistance of the electrodes. The open circuit was assumed when the electrical resistance of the fabricated electrode was >1 GΩ.

Fabrication of Microphotodetector. An active layer of a light harvesting mixture composed of P3HT and bis-phenyl C_{60}-butyric acid methyl ester (bis[60]PCBM) was deposited on the microelectrode. Briefly, 0.02 g of P3HT dissolved in 2 mL of *o*-dichlorobenzene was mixed with 0.016 g of bis[60]PCBM solution in 2 mL of *o*-dichlorobenzene. Three microliters of the active layer was deposited by spin-coating on the electrodes at 500 rpm for 10 s (step 1), followed by 1000 rpm for 10 s (step 2). The spin-coated surfaces were checked for uniformity using optical microscopy. The absorption, emission spectroscopy, and AFM were used to characterize the active layer of the microphotodetector devices.

LED Assembly on PLE-Fabricated Flexible Electrodes. The conductive flexible ITO-PET substrates (Delta Technologies) with dimensions of 4 mm × 13 cm were rinsed with ethanol and air-dried prior to the probe etching for the fabrication of electrodes. The film attached to a glass slide was placed on the *x*- and *y*-motorized stage of the microscope using a double-sided tape (3M). PLE hydrogel probes attached to a piezoelectric stage were soaked in an acidic solution of Fe(III) for at least 1 h prior to the experiment. The PLE was brought in contact to the conductive substrate. The stage was programmed to move with *x*- and *y*-speed (v_x and v_y) of 5 μm/s in a zig-zig pattern (175 μm in the *x*-direction, followed by 200 μm in the *y*-direction),

DOI: 10.1021/acsaelm.9b00099
ACS Appl. Electron. Mater. 2019, 1, 752−763

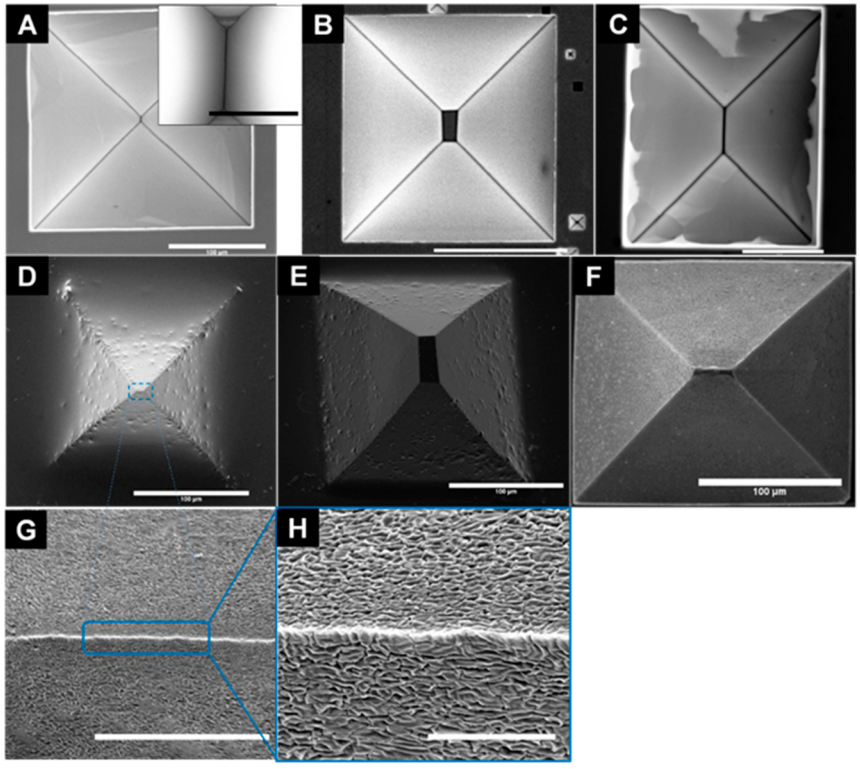

Figure 1. SEM of typical pyramidal pores and PAAM PLE probes. (A) SEM of line-shaped. Inset shows a larger magnification image of the tip, the tip width is roughly 50 nm (scale bar = 4 μm). (B, C) Pyramidal pores in Si wafers were fabricated using anisotropic etching of Si in basic solution. Corresponding nanoporous PAAM PLE probes of line-shaped (D) and rectangular-shaped (E, F) were formed by filling the pores up with PAAM solution and peeling them away from the Si wafer. Higher-resolution SEMs of (D) are shown in (G), and (H) shows that the tip is ~300 nm × 700 nm (scale bars are 10 and 5 μm, respectively). The scale bar is 100 μm for images (A)−(F).

that resulted in interdigitated electrodes for the fabrication of the microphotodetectors/LED assembly. The metal erasing was performed from edge-to-edge for an etched length of ~4 mm. The electrical resistance across the interdigitated electrodes yielded an open circuit system (>1GΩ), indicating that the conductive material in the patterned area was completely removed. Blue and green LEDs were glued to the film using silver paint, followed by putting a thin layer of super glue for mechanical stability. Copper tape was connected to the two electrodes on the flexible ITO substrates for attaching devices to an external power supply (GW INSTEK GPS-18500). A forward bias of 3.0 V was used for all LED experiments. Stretching studies on the flexible electrodes were carried out by mounting the LED−ITO−PET setup on an *x*-*y* stage. The LEDs glued using silver paint and copper tape on PLE-etched devices were then connected to a Keithley 6487 (applied potential (V_{appl}) = 3 V). Current and resistance measurements were monitored as the device was stretched with increments of 2 mm.

RESULTS AND DISCUSSION

Pyramidal Pores in Si Wafers. Figure 1 shows SEM images of the pyramidal pores obtained using Si anisotropic etching in an aqueous pyrocathecol−ethylenediamine mixture. The activation energy for alkaline etching of Si(100) planes is smaller than that of Si(111) planes,[52] which results in a higher etching rate for the Si(100) planes compared to the Si(111) planes. The size and shape of the pyramidal pore depend upon the shape and size of the exposed silicon during etching. The square-shaped exposed areas on photoresist-coated Si wafers resulted in sharp pointed pores when the etching was proceeded to completion. However, the square-shaped tip pyramidal pores resulted when the etching was stopped prior to its completion. Similarly, the rectangular-shaped exposed areas on the photoresist-coated Si wafers yielded sharp line or rectangular-shaped pores depending upon the extent of etching. For example, a line-shaped tip was obtained when the exposed area at the start of the etching was rectangular. However, stopping the etching process at an intermediate stage prior to a complete etching resulted in a rectangular tip pyramidal pore. Figure 1 shows both the line-shaped and rectangular-shaped pores in the Si wafer produced in our experiments. The tip (d_t) of the PLE probes ranged between 300 nm and 64 μm depending upon the extent of the Si(100) etching. A submicron PLE line-shaped probe that was 300 nm wide and 700 nm long was also prepared (Figures 1D,H). These sharp tips were used for the fabrication of the PAAM hydrogel probes for the high- resolution erasing applications.

Nanoporous hydrogel PLE probes were prepared by radical polymerization of AM (monomer, *M*) with bAM (cross-linker, *C*) in the presence of APS (initiator) and catalyst TEMED. The ratio of *C* to *M* (R_{MC}) was 0.2% in all PLE probes (eqs 1 and 2). In practice, both the storage capacity and mechanical properties of the probe need to be considered for patterning requirements. Therefore, the composition of the PLE probes should be carefully adjusted depending upon the erasing and writing requirements.

$$T(w/v) = \frac{M + C}{V} \times 100\% \quad (1)$$

$$C(w/w) = \frac{C}{M + C} \times 100\% \quad (2)$$

After cross-linking of the polymer in the pyramidal pores and subsequent peeling off from the Si wafer, an optically clear

DOI: 10.1021/acsaelm.9b00099
ACS Appl. Electron. Mater. 2019, 1, 752−763

Scheme 2. (A) Schematic of the Set-Up Used for PLE-Based Erasing[a], (B) the Relative Movement between the Substrate and PLE Probe Loaded with a Redox-Etchant Allowed for a Desired Pattern Formation, and (C) a Close-Up Image of the Meniscus Formed between the PLE Probe and the Substrate

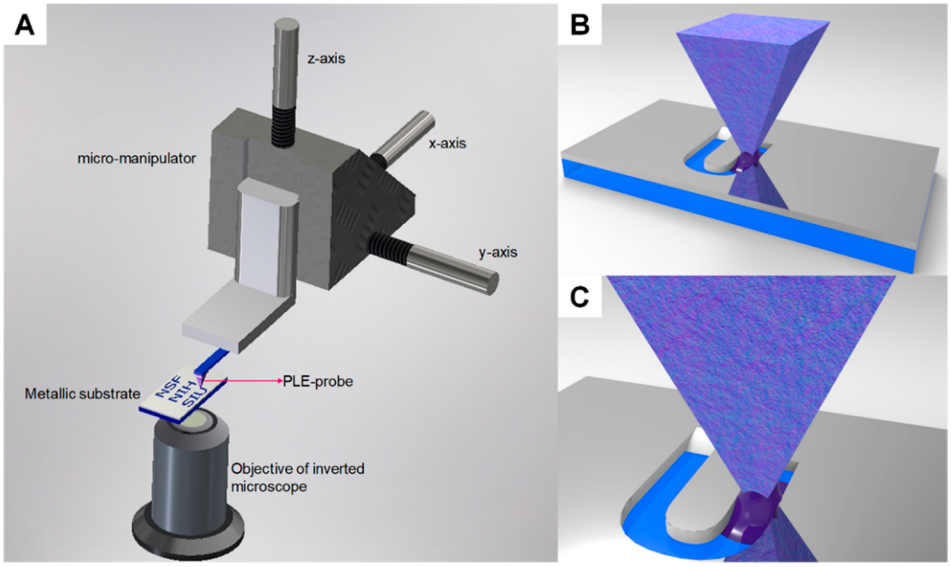

[a]The PLE probe is attached to a glass cantilever which is fixed to a piezoelectric micro-manipulator.

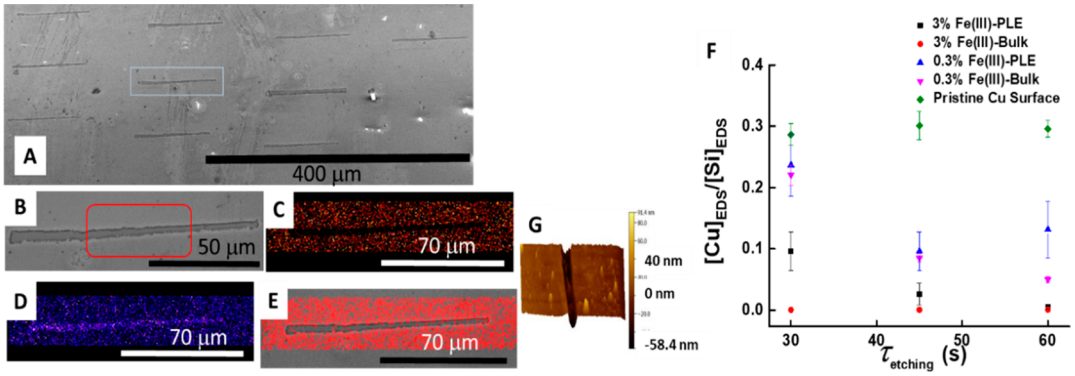

Figure 2. Copper erasing and pattern formation. PLE was used to erase copper and formation of patterns on copper surfaces for the fabrication of the microphoto-detectors. (A) An SEM of an array of rectangular-shaped Cu-erased patterns using a PLE probe. The electrochemical erasing was performed using a PLE probe with tip dimension of 500 nm × 110 μm; τ_e = 30s; RH = 40 ± 10%; T = 25 °C; and [Fe(III)] = 3%. The length and width of the erased patterns were 112 ± 2.5 μm and 2.7 ± 0.7 μm (n = 9), respectively. (B) A higher magnification SEM of an erased pattern in the blue rectangle in (A). The EDS mapping analysis shows complete depletion of the element Cu (C) with an increase in the Si signal (D). (E) An overlap of elemental Cu and Si signals. The comparison of the $R_{etching,vol} - \tau_{etching}$ for the PLE probe and bulk etching is shown in (F). $R_{etching,vol}$ for the PLE were 0.4 and 0.90 $\mu m^3/s$ for [Fe(III)] = 0.3 and 3%, respectively; whereas the bulk etching rate was four times larger for [Fe(III)] = 3%. (G) An AFM of an etched pattern with a depth of ∼45 nm.

array of polymer probes was yielded. Porous PAAM probes were imaged using SEM after lyophilization of the hydrogel for a closer visualization at a high spatial resolution of the porous matrix (Figures 1G,H). Although SEM provided nanoscale resolution of the pores, the pore size distribution within the PLE matrix from SEM images cannot accurately obtained. This is because of a low contrast limitation for our samples below 10 nm and a lack of high-resolution information deep inside of the PLE matrix. Further, the harsh vacuum conditions used during imaging also affected the pore and interpore dimensions. Finally, a thin conductive metal coating (∼10−15 nm) sputtered for SEM imaging may also damage or distort the sample at nanoscale. Due to these reasons, although the SEM information on the porous PLE is highly useful, the spatial information below 10 nm should be interpreted with caution.

Patterning Using PLE Electrochemical Metal Erasing. Patterning and deposition of metals to fabricate microelectronic components at the micro- and nanoscale frequently utilize wet chemical etching of noble metals, including Au, Ag, and Cu.[53] One reason for their extensive use in electronic and optoelectronic devices is their low electrical resistivity and relatively high chemical inertness to chemical attacks. Metal etching usually involves dissolution of metal using a liquid-phase etchant on selective parts of the metal; whereas a masked metal area is protected against the etching. The photoresist masked metal using photolithography followed by isotropic metal etching is shown to achieve a spatial resolution as high as 50 nm.[54]

Device miniaturization in the electronic industry demands development and enhancement in the state-of-the-art of tools and techniques for microfabrication. Several techniques,

DOI: 10.1021/acsaelm.9b00099
ACS Appl. Electron. Mater. 2019, 1, 752−763

including FIB,[55] are capable of meeting the industry requirements in terms of resolution, yet the multiplexing, throughput rate of these techniques is not implemented at the industrial scale for device fabrication. Further, in general, appropriate clean room facilities are required for the above-mentioned lithography and photolithographic patterning techniques, where submicron resolution is required. However, the equipment and maintenance costs (including, that of clean room) associated with the above-mentioned tools can be extremely high, which warrants for alternative fabrication tools that would help in lowering the cost of device fabrication.

In this report, PLE-based editing is demonstrated for on-demand etching and patterning of metal (Cu, Ag, and ITO) and other technologically important materials with features at microscale. Further, we also demonstrate here the fabrication of functional microphotodetectors and LED assembly on soft and hard surfaces that were patterned at microscale using PLE probes.

Electrochemical Copper Erasing Using PLE Probes. Fe(III) is industrially used for the etching of the Cu metal. Cu(0)/Fe(III) redox reaction provides water-soluble, predominantly, $FeCl_2^+$ and Cu(II) species.[56] The overall redox reaction usually represented by eq 3 is thermodynamically accessible (E_o = 0.43 V)

$$2Fe(III) + Cu(0) \rightarrow 2Fe(II) + Cu(II) \quad (3)$$

Importantly, redox reaction Cu(0)/Fe(III) is kinetically fast and follows the first-order rate constant with $R_{etching}$ = 0.2−0.33 mg Cu·kg/cm^2·s·mol Fe(III) for 0 < [Fe(III] < 0.8 mol/kg.[57,58]

Scheme 2 shows the setup used to perform PLE experiments. The PLE probe was attached to a glass cantilever that was then fixed to a piezoelectric stage (step size of 150 nm). By programming the *x*-*y* stage as described in the Materials section, a desired erasing pattern was achieved by delivering etchant molecules contained in the probe matrix to the substrate while moving the stage (Scheme 2B,C). Figure S2 shows the photographs of various parts of set-up used in the microscale erasing of various metallic surfaces for the device fabrication.

Figure 2 presents a line array patterns of ten electrochemical etched lines fabricated on an 100 nm copper-coated glass, using a rectangular PLE probe impregnated with Fe(III) (probe tip dimension was 500 nm × 110 μm). Figures S3 and S4 show EDS color mapping and spectra of PLE probes loaded with Ag, Cu, and ITO etchants. For line patterns formed in Figure 2, the Fe(III) etchant concentration, etching time (τ_e), relative humidity (RH), and temperature (T) were 3% (w/w), 30 s, 40 ± 10%, and 25 °C, respectively. The width and length of the line-shaped patterns were 2.7 ± 0.7 μm and 112 ± 2.5 μm (n = 9), respectively, suggesting the microscale features with a narrow-etched pattern distribution can be obtained using PLE probes in wet lab settings.

It is noticeable, that the size of the patterned features is larger than the tip dimension. For example, the patterns formed in these studies were about five times wider (~2.7 μm) than the width of the PLE probe tip of 500 nm (Figure 2). This is consistent with our previous studies, where the PLE-fabricated patterns were also larger than the size of the probe.[59] The contribution of various factors, including meniscus size at tip−substrate interface, molecular interaction between the tip and surface, mechanical properties of the probe tip, and ink-transport characteristics, ultimately determine the size of the patterned features.[34] Further, parameters, such as relative humidity, temperature, and ink physicochemical characteristics, also contribute to the formation and size of the water meniscus.[60]

In Scheme 2C, the meniscus at the PLE probe−substrate interface is shown for illustrative purposes. However, at this point, we do not know the exact size of the meniscus at the PLE tip−substrate interface. However, we estimate the meniscus at the tip−substrate interface larger than the size of the tip. The erasing process is through a diffusion-based mechanism, where the redox etchant from the PLE probe transports etchant to the substrate.[59] Thus, the PLE erasing is similar to DPN lithography, where the solvated ink molecules diffused to the patterning surface through the meniscus at the tip−substrate interface. Finally, the erasing pattern size using PLE etching depends upon many experimental parameters and probe and ink characteristics (please see above for more discussion). More detailed studies are needed to fully understand the contributions of each parameter on the erasing pattern dimension.

Cu etching with PLE probes was also confirmed by EDS and AFM analysis. EDS elemental Cu and Si concentrations represented by $[Cu]_{EDS}$ and $[Si]_{EDS}$ in the EDS mapping confirmed the depletion of Cu (Figure 2B−E). The orange- and purple-shaded EDS maps show elemental Cu and Si, respectively (Figure 2C,D); whereas the elemental Cu and Si overlap is shown in Figure 2E. Under our experimental conditions, the electrochemical Cu(0)/Fe(III) redox reaction was dependent upon both the etching time ($\tau_{etching}$) and Fe(III) concentration. Figure 2F shows that decrease in the $^{[Cu]_{EDS}}/_{[Si]_{EDS}}$ ratio with $\tau_{etching}$ for both [Fe(III)] = 0.3 and 3% conditions. $^{[Cu]_{EDS}}/_{[Si]_{EDS}} \approx 0.1$ suggested that copper was not completely etched, but it remained constant for $\tau_{etching}$ > 45s and [Fe(III)] = 0.3% (Figure 2). The etching rate of Cu(0) was found to increase with [Fe(III)] = 3% containing PLE probes; a complete Cu etching was observed for $\tau_{etching}$ = 60s, as confirmed using EDS. The quantitative Cu(0) volumetric etching rate ($R_{vol,etching}$) was followed by AFM measurements (Figure 2G). $R_{vol,etching} = \frac{\partial A \times d_f}{\partial t}$ was estimated by erased metal area (∂A) from SEM measurements, known thickness (d_f = 100 nm) of the coating, and erasing time. We estimated $R_{vol,etching} \approx 0.5$ and 1.0 μm^3/s with [Fe(III)] = 0.3 and 3%, respectively, for a rectangular-shaped PLE probe with dimensions of 500 nm × 110 μm.

We performed additional experiments to study the etching rates of the copper in bulk conditions and compared this with PLE probe etching. We found that the etching rate was more than four times faster in the bulk solution for [Fe(III)] = 3% as compared to the PLE etching ([Fe(III)] = 3%, Figure 2F). However, there were insignificant differences in the etching rates between PLE-based and bulk etching for [Fe(III)] = 0.3%. These results imply that there are differences between the PLE-probe and bulk etching rate depending upon the etchant conditions, and that the PLE locomotion speed needs to be adjusted for optimum etching. Although more thorough studies are needed to investigate why this difference would be. One of the possibilities is that at higher etchant conditions beyond a limiting value for the bulk case, the local etchant concentration and mass transport are sufficiently high and allowed for the enhanced etching rate in comparison to the PLE-based etching. Additionally, we also investigated the

DOI: 10.1021/acsaelm.9b00099
ACS Appl. Electron. Mater. 2019, 1, 752−763

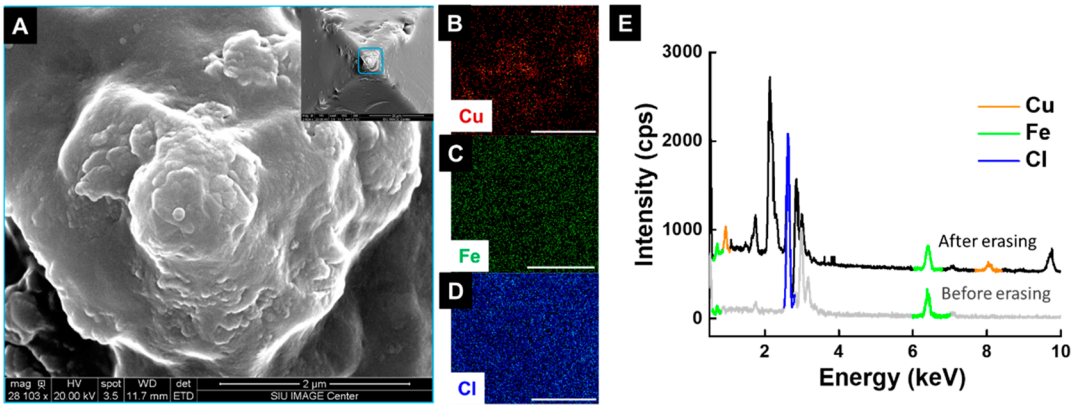

Figure 3. (A) A higher magnification SEM image of a PLE tip loaded with [Fe(III)] = 0.3% after Cu etching (magnification, ~28 k; scale bar = 2 μm). Inset of (A) shows a lower magnification image. EDS color mapping in the PLE probe with Cu (B, maroon), etchant molecules Fe (C, green), and Cl (D, blue); scale bars = 2 μm. (E) The EDS spectrum obtained at the tip of the PLE probe before (bottom) and after (top) Cu etching. Energy peaks at 2.98 (Ag Lα), 2.12 (Au M), 9.712 (Au Lα), and 2.828 keV (Pd Lα) came from conductive coating performed on the PLE probe. The presence of the Cu X-ray peaks in the spectrum suggested the diffusion of the aqueous copper species into the porous PLE probe.

mechanical stability of the polymer PLE probes. After utilizing the PLE probes for three erasing cycles with >30 000 μm^2 Cu erasing, insignificant damage to the probe was evident from the SEM imaging.

The coating thickness employed in the microelectronics, batteries, and other devices is comparable to those employed here, suggesting that the results in these studies are relevant to the etching of conductive coatings employed in the microelectronics and other related industries. Importantly, we routinely and reproducibly obtained spatial features of <10 μm in width and up to many cm in length using PLE probes. These results are useful for device fabrication because of the microscale-erased feature dimension we can obtain at a relatively high throughput rate. With optimization of the PLE probe and etching conditions (etching time, temperature, and etchant concentration), finer etching patterns of submicron dimensions with appropriate high throughput rates are feasible.

An interesting question arises when metal is removed from the substrate during PLE erasing, what is the fate of the reaction products following the erasing process? In the PLE process, erasing is performed at the probe−substrate interface through an electrochemical reaction between an etchant and metal (M(0)). The formation of solvated M^{n+} through the redox reaction allows for erasing of M(0). The solvated M^{n+} ions diffuse into the probe and to the surrounding areas. In order to address this question, EDS and SEM were used to examine the PLE probe before and after copper etching. A total area of ~28 716 μm^2 was etched using [Fe(III)] = 0.3% and RH = 40% at 25 °C. A low etchant concentration in the PLE probe and a large surface erasing were found to be suitable for investigating the fate of solvated Cu(II) after the erasing process. Erasing of small areas (<10 000 μm^2) was not successful in the detection of solvated Cu(II) in the PLE probe, probably due to the EDS detection limit and low concentration of the Cu(II) into the probe.

The EDS spectra gathered at the tip of the PLE probe showed accumulation of Cu speciation after etching within the PLE matrix (Figure 3). Fe Kα and Lα with energies of 6.398 and 0.705 keV, respectively, and that of Cl Kα of 2.621 keV are shown in Figure 3E. The energy peaks of 0.93 and 8.04 keV, corresponding to Cu Lα and Kα peaks, respectively, confirmed the presence of Cu in the PLE probe (Figure 3E). It is important to note, that the EDS analysis is semiquantitative in the present studies. Therefore, we cannot overemphasize the EDS data presented here; although, qualitatively, EDS results provided a clear evidence of erased Cu species in the probe. Further, at this point, it is not entirely clear if all the solvated Cu species diffused into the probe. More extensive quantitative studies are underway to clarify these questions and will be reported in a future article.

The diffusion of the reaction products into the PLE matrix can have an implication on the erasing process. In the initial stage, the effect of the diffusion of the products into the PLE matrix is expected to be low because the etchant concentration difference (which is the driving force) is large for the etchant to diffuse out of the probe. Also, the low product concentration is expected to have an insignificant effect on the erasing rate. However, large area erasing may significantly increase the reaction product concentration in polymer matrix, which, in principle, can hinder the etchant diffusion out of the probe to the meniscus present at the probe−substrate interface. It appears that careful studies are needed to fully understand the effect of diffusion of the reaction products on PLE erasing.

Translocation of PLE Probes for Metal Patterning. Whereas Cu etching in the previous section was accomplished using the PLE probe−copper surface contact, the relative motion between the PLE and the substrate was demonstrated for patterning on Ag and ITO surfaces. Figure S5 shows the microscale Ag erasing patterns accomplished by moving [I_2 − KI] = 18% (w/v), containing PLE probes at a speed of 5 μm/s. A rectangular-shaped PLE probe (dimension = 11 μm × 24 μm) was used for these experiments. The SEM and EDS measurements of the erased patterns indicated that the complete removal of Ag from the surface was achieved after two probe passes (cycles) over the pattern. One PLE erasing cycle did not appear to etch Ag completely, but ~97% silver remained on the surface after one erasing cycle. The EDS mapping of elemental Ag and Si confirmed complete erasing after three or more erasing PLE cycles (Figure S6). Patterns with width and length ~32.2 ± 11.6 μm and ~1330 μm (1.33 mm), respectively, and an erased area of ~0.043 mm^2 were accomplished, which yielded an areal speed ($R_{area,etching}$) and $R_{vol,etching}$ of ≈80 and 8 $\mu m^3/s$, respectively. $R_{area,etching} = wxv_{probe}$ and $R_{vol,etching} = wxv_{probe} \times d$; here, w, d, and v_{probe} are the width of the pattern, thickness of silver coating, and speed

DOI: 10.1021/acsaelm.9b00099
ACS Appl. Electron. Mater. 2019, 1, 752−763

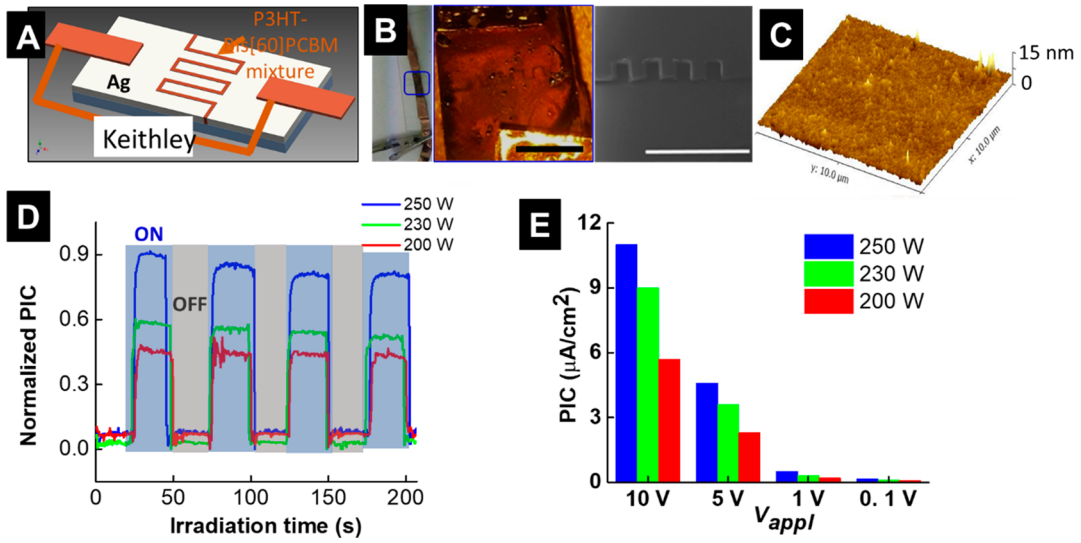

Figure 4. Microphotodetector fabricated using PLE-based patterning of silver interdigitated electrodes. (A) A schematic of a microphotodetector prepared by erasing silver in a zigzag pattern, thereby fabricating an interdigitated electrode and spin coating an electron donor−acceptor pair on the electrode (brown zigzag line). Two copper electrodes were attached to the pattern substrate and connected to electric potential using Keithley 6487. (B) The optical photograph (left) and higher magnification optical photograph (middle) of a microphotodetector assembly in the blue square. The zigzag patterns on the electrodes are visible in (B). The dark-reddish color comes from the deposition of the donor−acceptor mixture. An SEM image of the patterned electrode (right, scale bar 2 mm). (C) An AFM of the P3HT−bis[60]PCBM mixture deposited on the photodetector. (D) A typical PIC-time response of the microphotodetector for three different powers (200, 230, and 250 W). The measured photon intensity at 534 nm (Newport Model, 818-SL) for 200, 230, and 250 W were 142, 220, and 240 mW/cm^2, respectively. (D) Normalized PIC-V_{appl} dependence for the microphotodetector at three different photon intensities.

of the probe, respectively. Assuming complete Ag erasing was accomplished in two erasing cycles (Figure S6) at v_{probe} = 5 μm/s, the observed Ag $R_{vol,etching}$ was ∼8 times that of $R_{vol,etching}$ for the Cu where the PLE probe−surface contact mechanism was employed. The $R_{vol,etching}$ depends upon the probe size, concentration, and temperature of the redox etchant and etchant-metal redox kinetics rate. For example, a larger probe size delivers a larger volume of the etchants that will result in enhanced $R_{vol,etching}$. Similarly, as shown for the Cu etching, the etchant concentration is also an important parameter that affects the etching rate. In our experiments, the area of the PLE probe used for the Ag erasing was ∼5 times larger than the area of the probe used for the Cu etching, which may account for the enhanced etching rate. Further, the etchant-metal redox kinetics consideration is also important for full utilization of the probe-based pattern formation. Under optimized conditions, a larger etching rate than those demonstrated here can be obtained by controlling the etchant concentration and temperature, probe dimension, and mass-transport and kinetics of the metal-etchant reaction.

Fabrication of Functional Microphotodetector and LED Devices Using PLE Patterned Electrodes. The interdigitated electrodes were fabricated by translocating the 18% w/v aqueous [KI−I_2]-complex containing PLE probes over Ag-coated glass wafers at a speed of 5 μm/s. Figure 4A shows a schematic of the interdigitated electrode-based microphotodetector fabricated using the PLE erasing. The zigzag probe movement of the PLE over the metallic coating resulted in interdigitated electrodes with a conductive metal electrode width and spacing of 50 and 150 μm, respectively (inset Figure 4B). After Ag etching, the electrical resistance of the electrode increased from <10 Ω to >1 GΩ (reliable limiting electrical resistance of our multimeter was 1 GΩ), suggesting that the Ag erasing was successful. These results were also confirmed by the EDS measurements (Figure S6). Electron donor−acceptor pairs of P3HT and bis[60]PCBM of 1 and 0.8% concentrations, respectively, were spin-coated on the interdigitated electrodes. The films composed of only P3HT and bis[60]PCBM and that of the P3HT-bis[60]PCBM mixture were also characterized using AFM (Figures S7 and 4C). The emission spectra of P3HT before and after addition of the acceptor in the solution phase indicated an emission quenching efficiency of ∼45% (Figure S8). These results are consistent with previous studies, suggesting strong donor−acceptor interactions and charge transfer between excited state P3HT and bis[60]PCBM.[61] Figure 4B shows the experimental set-up used for the acquisition of PIC). Figure 4D shows typical PIC-time responses of a typical microphotodetector device with the light "ON" and "OFF". A solar simulator (AM 1.5) under ambient wet laboratory conditions was used for all photoinduced studies. With photon irradiation, the PIC increases sharply, exhibiting both the rise (τ_{rise}) and decay times (τ_{decay}) < 500 ms. The device response was found to be stable for less than five "ON−OFF" cycles; the PIC signal response decreased significantly after >10 cycles. This decrease in the PIC signal is attributed to photodegradation of the active organic layer.

Fabrication and testing of devices were performed in wet lab conditions in air (21% oxygen and humidity between ∼50%). Oxygen is singlet in its ground state and is an excellent quencher for molecules in the excited state.[62] Both P3HT and PCBM are known to oxidize and degrade under photo-irradiation conditions. Specifically, the photodegradation of P3HT is a light-initiated radical mechanism, where the concentration of the quenched sites increases with the photo-oxidation.[63] Similarly, PCBM can undergo a series of oxidation when photoradiated, which acts as electron traps, as shown by experimental and DFT studies.[64] The degradation of the performance of the devices such as ours can be minimized by hermetically sealing the devices with materials that

DOI: 10.1021/acsaelm.9b00099
ACS Appl. Electron. Mater. 2019, 1, 752−763

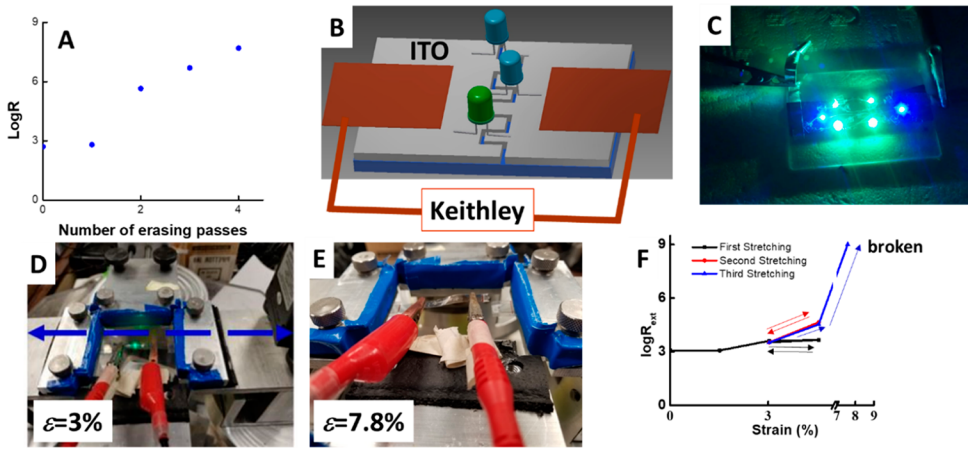

Figure 5. Testing of the LED assembly on the PLE-fabricated ITO electrodes. (A) Log*R*-number of erasing passes dependence for the ITO electrodes. Here, *R* represents the electric resistance of the ITO electrode as a function of number of PLE erasing cycles. (B) Schematic of an LED assembly on ITO electrodes. (C) Four green and two blue LEDs assembled on an electrode fabricated across an ITO electrode that was fabricated using locomotion of a PLE probe impregnated with acidic Fe(III). The optical photographs of the LED devices assembled on flexible electrodes that were stretched with ε = 3 (D) and 7.8% (E). (F) LogR_{ext}-ε dependence indicated that the electrical resistance was not affected significantly for ε = 3.3, but the R_{ext} increased exponentially at ε > 4.5%. The device was damaged at ε = 7.5%.

eliminate (or significantly reduce) the transport of oxygen, water, and other performance degrading species.

Interestingly, the PIC signal depends on the photoexcitation power (P) and the applied voltage (V_{appl}) across two electrodes. PIC-photoexcitation power and PIC-V_{appl} dependences are shown in Figure 4D,E respectively. In general, higher photon intensity consistently resulted in larger PIC. For example, PIC was ∼2 times that when P = 250 W than when P = 200 W. The PIC enhancement at a higher lamp power is attributed to an increase in photocharge generation, leading to enhanced PIC. More dramatic PIC-V_{appl} dependence was observed under the same photon intensity conditions (Figure 4D). For example, $PIC_{10,1} = \frac{PIC_{10}}{PIC_1}$ was >20 for all the photon intensities (200, 230, and 250 W) tested under our experimental conditions. $PIC_{10,1}$ is a measure of the influence of applied potential, and it is defined as the ratio of PIC at V_{appl} = 10 V to PIC at V_{appl} = 1 V. Similarly, $PIC_{5,1}$ and $PIC_{1,0.1}$ were >9 and >2.5, respectively, for our experimental conditions. In fact, $PIC_{10,0.1}$ > 65 for all the photon power tested in our experiments. The strong PIC-V_{appl} dependence is not surprising for randomly dispersed donors and acceptors in the inhomogeneous film where the significant losses due to charge recombination and charge trapping and other charge loss mechanisms exist.[65] The application of an external electric field drastically decreased the charge recombination and other losses in the device by forcing the electrons and holes to transport to opposite appropriate electrodes, thereby, dramatically enhancing the PIC signal at higher V_{appl}.

LED Device Assembly on Flexible Electrodes. ITO-coated flexible polyester (PET) substrates (1 cm × 2.7 cm) were also patterned using PLE probes soaked in acidic 0.2 M Fe(III). Etching of ITO with acidic Fe(III) is thermodynamically favorable with a reported activation energy of 56 ± 5 kJ/mol.[66] The Fe(III) containing PLE probes were translocated at a speed of 5 μm/s over the ITO surface. Under these experimental conditions, multiple PLE probe erasing cycles were needed to completely etch ITO from the surface. The electrical resistance-number of erasing cycles dependence is shown in Figure 5A. The electric resistance (R) of the ITO surface increased from 500 Ω to >50 MΩ after four erasing passes for an etched line of ∼200 μm × 1 cm line, suggesting successful ITO erasing (Figure 5A). A schematic and a typical working device with six LEDs (four green and two blue) mounted on the PLE-etched ITO substrate are shown in Figure 5B,C, respectively. We examined the working behavior of an LED assembled on a flexible ITO−PET substrate by mounting it on a mechanical station for stretching experiments (Figures 5D,E and S9). Stretching and relaxation of the unstrained state in the first cycle did not result in a significant change in electrical resistance (R_{ext}) under strain (ε) up to ε up to 4.5% (two-way black arrows) (Figure 5F). A second stretching cycle with ε = 4.5% (two-way red arrows) led to an increase in R_{ext} by an order of magnitude which returned to the original value after being relaxed to ε = 3%, showing limited electrical reversibility of the PLE-fabricated devices on ITO-coated polyester substrates. For ε = 7.6%, however, R_{ext} > 1 GΩ was observed. This is due to tearing of the ITO−PET substrates, which resulted in the destruction of the conductive pathways for charge transport through the devices.

The performance of the devices fabricated in this study was limited by the short-range extension failure due to material selection. With appropriate selection of base materials, such as PDMS or PDMS−urethane composites, Rogers and Bao's groups recently demonstrated working devices that can be stretched with a larger strain ε values up to or >250%.[43,45,67] More extensive studies are currently underway for the fabrication of highly stretchable functional devices based on PLE for wearable pressure and motion sensing applications.

It is instructive to discuss the PLE in light of other lithography techniques widely used in the industry and academia. The surface selective patterning can be accomplished using many currently available tools, including coated-AFM tips, focused ion beam (FIB), and electron beam lithography (EBL). For example, the selective removal of materials from a surface using AFM tips is demonstrated in the literature.[68] Importantly, AFM can remove materials from a surface through a mechanical process. However, this causes damage to the probe because of the physical contact between the tip and the surface, and the probe may need to be replaced if it is blunt due to damage. Similarly, FIB and electron

DOI: 10.1021/acsaelm.9b00099
ACS Appl. Electron. Mater. 2019, 1, 752−763

lithography allow for removal of materials and patterning at a high-resolution (<100 nm). However, the equipment and operating cost of these two instruments is high; many institutes and resource-limited countries cannot afford these expensive instruments. The PLE probe utilizes polymer and contains a liquid interface meniscus that reduces the friction during the locomotion of the probe. However, as demonstrated in this and in a previous article,[59] an electrochemical reaction facilitates the erasing process which can be many orders faster than the mechanical erasing of hard materials. Because a chemical reaction is performed at the microscale, a large number of materials are accessible for erasing at microscale. Further, multiple materials can be erased simultaneously, or a given material within a matrix of a composite made up of many species can also be erased. This opens new possibilities for fabricating new materials with spatial control at the microscale level. Finally, the usage of a hydrogel ensures that the amount of ink enclosed within the polymeric matrix is several orders of magnitude higher than the dry weight of the polymer.

It is also important to consider the resolution and throughput rate of erasing using AFM, FIB, EBL, and that of PLE probes. The resolution of writing and erasing using AFM, FIB, and an EBL is 2−3 orders better than the patterns made using the PLE probes. This is a direct consequence of the difference between the AFM and PLE probe size.[59] Similarly, the electron and ion beams in FIB and EBL, respectively, allow for a much higher resolution erasing than that demonstrated in this study. Further studies may allow for a decrease in the erasing features using PLE (probably through a sharper tip and through control of the experimental conditions). Additionally, the meniscus characteristics and experimental parameters, such as humidity, also influence the feature size of the patterns. The throughput rate (erasing and deposition rate) of the PLE-based patterning is many orders of magnitude larger than those patterns composed using AFM, FIB, and EBL tools. This is because of the large differences in the probe/beam size. Finally, the erasing process demonstrated in this report is accomplished using an electrochemical reaction at a much larger area, which is practically impossible to accomplish using AFM-based probes with the same erasing speed. Overall, PLE along with AFM, FIB, and EBL provide complementary tools for patterning and erasing patterns at nano- and micro-scale for potential applications in a wide range of fields, including microelectronics, biosensors, medical, and life-science.

CONCLUSIONS

We demonstrated the fabrication of functional devices based on interdigitated electrodes synthesized using probe-based etching of metallic coatings. Three different metallic coatings (Ag, Cu, and ITO) on both hard and soft surfaces were erased and patterned using diffusion-based etchant delivery to the metal coating in the contact mode between the substrate and PLE. The translocation of PLE allowed microscale electrochemical erasing (etching) of metallic coating on demand in an one-step process. On the basis of the etchant concentration, PLE probe speed, and metal thickness, the microscale erasing feature with a minimum pattern size of 2.7 μm was accomplished with an etching rate of ∼8 $\mu m^3/s$. Functional microphotodetector and LED assemblies were fabricated on flexible and hard conductive interdigitated electrodes composed using PLE probes. Overall, the PLE allowed for on-demand fast patterning of films of multiple metals with microscale features on both the soft and hard substrates for the fabrication of functional devices.

ASSOCIATED CONTENT

Supporting Information

The Supporting Information is available free of charge on the ACS Publications website at DOI: 10.1021/acsaelm.9b00099.

Scanning electron and optical micrographs of Si chip during photolithographic process, detailed description of photolithography and Si anisotropic etching, SEM and EDS mapping/spectrum of PAAM pen editor loaded with etchants, SEM and EDS mapping of erased patterned silver using commercial etchant, silver removal efficiency in atomic % obtained using EDS, AFM characterization of PCBM and P3HT films, absorption and emission spectrum of P3HT and composite P3HT:PCBM, and photograph of the mechanical stage used for mechanical tests (PDF)

AUTHOR INFORMATION

Corresponding Author

*E-mail: pkohli@chem.siu.edu.

ORCID

Punit Kohli: 0000-0003-3183-4385

Funding

National Science Foundation grants CHE 0748676, CHE 0959568, and DMR 1757954 and National Institutes of Health (GM 106364). C.O. and M.B. were supported through an NSF-REU award (DMR 1757954).

Notes

The authors declare no competing financial interest.

ACKNOWLEDGMENTS

We would like to thank Prof. Kyle Plunkett for providing us a sample of P3HT and Prof. P. Sivakumar for the use of his photometer. We also thank anonymous reviewers for their constructive comments that made the manuscript stronger.

REFERENCES

(1) Salaita, K.; Wang, Y.; Mirkin, C. A. Applications of dip-pen nanolithography. *Nat. Nanotechnol.* **2007**, *2*, 145.

(2) Piner, R. D.; Zhu, J.; Xu, F.; Hong, S.; Mirkin, C. A. "Dip-Pen" nanolithography. *Science (Washington, DC, U. S.)* **1999**, *283* (5402), 661−3.

(3) Ginger, D. S.; Zhang, H.; Mirkin, C. A. The evolution of dip-pen nanolithography. *Angew. Chem., Int. Ed.* **2004**, *43* (1), 30−45.

(4) Braunschweig, A. B.; Huo, F.; Mirkin, C. A. Molecular printing. *Nat. Chem.* **2009**, *1* (5), 353−8.

(5) Eichelsdoerfer, D. J.; Liao, X.; Cabezas, M. D.; Morris, W.; Radha, B.; Brown, K. A.; Giam, L. R.; Braunschweig, A. B.; Mirkin, C. A. Large-area molecular patterning with polymer pen lithography. *Nat. Protoc.* **2013**, *8* (12), 2548−60.

(6) Huo, F.; Zheng, Z.; Zheng, G.; Giam, L. R.; Zhang, H.; Mirkin, C. A. Polymer pen lithography. *Science (Washington, DC, U. S.)* **2008**, *321* (5896), 1658−60.

(7) Hedrick, J. L.; Brown, K. A.; Kluender, E. J.; Cabezas, M. D.; Chen, P. C.; Mirkin, C. A. Hard Transparent Arrays for Polymer Pen Lithography. *ACS Nano* **2016**, *10* (3), 3144−8.

(8) Xia, Y.; Whitesides, G. M. SOFT LITHOGRAPHY. *Annu. Rev. Mater. Sci.* **1998**, *28* (1), 153−184.

(9) Kim, K.-H.; Moldovan, N.; Espinosa, H. D. A Nanofountain Probe with Sub-100 nm Molecular Writing Resolution. *Small* **2005**, *1* (6), 632−635.

DOI: 10.1021/acsaelm.9b00099
ACS Appl. Electron. Mater. 2019, 1, 752−763

(10) Loh, O. Y.; Ho, A. M.; Rim, J. E.; Kohli, P.; Patankar, N. A.; Espinosa, H. D. Electric field-induced direct delivery of proteins by a nanofountain probe. *Proc. Natl. Acad. Sci. U. S. A.* **2008**, *105* (43), 16438.
(11) Moldovan, N.; Kim, K.-H.; Espinosa, H. D. Design and fabrication of a novel microfluidic nanoprobe. *J. Microelectromech. Syst.* **2006**, *15* (1), 204−213.
(12) Rogers, J. A.; Nuzzo, R. G. Recent progress in soft lithography. *Mater. Today* **2005**, *8* (2), 50−56.
(13) Menard, E.; Meitl, M. A.; Sun, Y.; Park, J.-U.; Shir, D. J.-L.; Nam, Y.-S.; Jeon, S.; Rogers, J. A. Micro- and Nanopatterning Techniques for Organic Electronic and Optoelectronic Systems. *Chem. Rev.* **2007**, *107* (4), 1117−1160.
(14) Lenhert, S.; Sun, P.; Wang, Y.; Fuchs, H.; Mirkin, C. A. Massively Parallel Dip-Pen Nanolithography of Heterogeneous Supported Phospholipid Multilayer Patterns. *Small* **2007**, *3* (1), 71−75.
(15) Wang, W. M.; Stoltenberg, R. M.; Liu, S.; Bao, Z. Direct Patterning of Gold Nanoparticles Using Dip-Pen Nanolithography. *ACS Nano* **2008**, *2* (10), 2135−2142.
(16) Corletto, A.; Yu, L.; Shearer, C. J.; Gibson, C. T.; Shapter, J. G. Direct-Patterning SWCNTs Using Dip Pen Nanolithography for SWCNT/Silicon Solar Cells. *Small* **2018**, *14* (16), No. 1800247.
(17) Huang, L.; Braunschweig, A. B.; Shim, W.; Qin, L.; Lim, J. K.; Hurst, S. J.; Huo, F.; Xue, C.; Jang, J. W.; Mirkin, C. A. Matrix-assisted dip-pen nanolithography and polymer pen lithography. *Small* **2010**, *6* (10), 1077−81.
(18) Kumar, R.; Weigel, S.; Meyer, R.; Niemeyer, C. M.; Fuchs, H.; Hirtz, M. Multi-color polymer pen lithography for oligonucleotide arrays. *Chem. Commun.* **2016**, *52* (83), 12310−12313.
(19) Kumar, R.; Bonicelli, A.; Sekula-Neuner, S.; Cato, A. C.; Hirtz, M.; Fuchs, H. Click-Chemistry Based Allergen Arrays Generated by Polymer Pen Lithography for Mast Cell Activation Studies. *Small* **2016**, *12* (38), 5330−5338.
(20) Xie, Z.; Chen, C.; Zhou, X.; Gao, T.; Liu, D.; Miao, Q.; Zheng, Z. Massively Parallel Patterning of Complex 2D and 3D Functional Polymer Brushes by Polymer Pen Lithography. *ACS Appl. Mater. Interfaces* **2014**, *6* (15), 11955−11964.
(21) Chung, S.-W.; Ginger, D. S.; Morales, M. W.; Zhang, Z.; Chandrasekhar, V.; Ratner, M. A.; Mirkin, C. A. Top-Down Meets Bottom-Up: Dip-Pen Nanolithography and DNA-Directed Assembly of Nanoscale Electrical Circuits. *Small* **2005**, *1* (1), 64−69.
(22) Lee, T.-W.; Jeon, S.; Maria, J.; Zaumseil, J.; Hsu, J. W. P.; Rogers, J. A. Soft-Contact Optical Lithography Using Transparent Elastomeric Stamps and Application to Nanopatterned Organic Light-Emitting Devices. *Adv. Funct. Mater.* **2005**, *15* (9), 1435−1439.
(23) O'Connell, C. D.; Higgins, M. J.; Moulton, S. E.; Wallace, G. G. Nano-bioelectronics via dip-pen nanolithography. *J. Mater. Chem. C* **2015**, *3* (25), 6431−6444.
(24) Mirkin, C. A.; Hong, S.; Demers, L. Dip-pen nanolithography: controlling surface architecture on the sub-100 nm length scale. *ChemPhysChem* **2001**, *2* (1), 37−39.
(25) Hwang, K.; Shin, C.; Mingwu, R.; Lee, S.-H.; Kim, H.-m. Design of a nano-printer based on AFPN (Active Fountain Pen Nano-lithography) using switch control. *Journal of Mechanical Science and Technology* **2011**, *25* (4), 977−985.
(26) Zhang, H.; Elghanian, R.; Amro, N. A.; Disawal, S.; Eby, R. Dip Pen Nanolithography Stamp Tip. *Nano Lett.* **2004**, *4* (9), 1649−1655.
(27) Liao, X.; Braunschweig, A. B.; Mirkin, C. A. "Force-feedback" leveling of massively parallel arrays in polymer pen lithography. *Nano Lett.* **2010**, *10* (4), 1335−1340.
(28) Jaeger, R. D.; Gleria, M. *Inorganic polymers*; Nova Science Publishers: New York, 2007.
(29) Eichelsdoerfer, D. J.; Brown, K. A.; Wang, M. X.; Mirkin, C. A. Role of Absorbed Solvent in Polymer Pen Lithography. *J. Phys. Chem. B* **2013**, *117* (50), 16363−16368.
(30) Senesi, A. J.; Rozkiewicz, D. I.; Reinhoudt, D. N.; Mirkin, C. A. Agarose-Assisted Dip-Pen Nanolithography of Oligonucleotides and Proteins. *ACS Nano* **2009**, *3* (8), 2394−2402.
(31) Liu, G.; Zhou, Y.; Banga, R. S.; Boya, R.; Brown, K. A.; Chipre, A. J.; Nguyen, S. T.; Mirkin, C. A. The role of viscosity on polymer ink transport in dip-pen nanolithography. *Chemical Science* **2013**, *4* (5), 2093−2099.
(32) Xia, Y.; Whitesides, G. M. SOFT LITHOGRAPHY. *Annu. Rev. Mater. Sci.* **1998**, *28* (1), 153−184.
(33) Schwartz, P. V. Molecular Transport from an Atomic Force Microscope Tip: A Comparative Study of Dip-Pen Nanolithography. *Langmuir* **2002**, *18* (10), 4041−4046.
(34) Urtizberea, A.; Hirtz, M.; Fuchs, H. Ink transport modelling in Dip-Pen Nanolithography and Polymer Pen Lithography. *Nano-fabrication* **2016**, *2*, 1.
(35) Wang, X.; Wang, X.; Fernandez, R.; Ocola, L.; Yan, M.; La Rosa, A. Electric-Field-Assisted Dip-Pen Nanolithography on Poly(4-vinylpyridine) (P4VP) Thin Films. *ACS Appl. Mater. Interfaces* **2010**, *2* (10), 2904−2909.
(36) Amro, N. A.; Xu, S.; Liu, G.-Y. Patterning Surfaces Using Tip-Directed Displacement and Self-Assembly. *Langmuir* **2000**, *16* (7), 3006−3009.
(37) Liu, M.; Amro, N. A.; Liu, G.-Y. Nanografting for Surface Physical Chemistry. *Annu. Rev. Phys. Chem.* **2008**, *59* (1), 367−386.
(38) Li, Y.; Maynor, B. W.; Liu, J. Electrochemical AFM "Dip-Pen" Nanolithography. *J. Am. Chem. Soc.* **2001**, *123* (9), 2105−2106.
(39) Tinazli, A.; Piehler, J.; Beuttler, M.; Guckenberger, R.; Tampé, R. Native protein nanolithography that can write, read and erase. *Nat. Nanotechnol.* **2007**, *2* (4), 220−225.
(40) Rajasekaran, P. R.; Zhou, C.; Dasari, M.; Voss, K.-O.; Trautmann, C.; Kohli, P. Polymeric lithography editor: Editing lithographic errors with nanoporous polymeric probes. *Science Advances* **2017**, *3* (6), e1602071.
(41) Khang, D.-Y. A Stretchable Form of Single-Crystal Silicon for High-Performance Electronics on Rubber Substrates. *Science (Washington, DC, U. S.)* **2006**, *311*, 208.
(42) Kim, D.-H.; Ahn, J.-H.; Choi, W. M.; Kim, H.-S.; Kim, T.-H.; Song, J.; Huang, Y. Y.; Liu, Z.; Lu, C.; Rogers, J. A. Stretchable and Foldable Silicon Integrated Circuits. *Science (Washington, DC, U. S.)* **2008**, *320* (5875), 507−511.
(43) Kim, D.-H.; Ghaffari, R.; Lu, N.; Rogers, J. A. Flexible and Stretchable Electronics for Biointegrated Devices. *Annu. Rev. Biomed. Eng.* **2012**, *14* (1), 113−128.
(44) Kunnavakkam, M. V.; Houlihan, F. M.; Schlax, M.; Liddle, J. A.; Kolodner, P.; Nalamasu, O.; Rogers, J. A. Low-cost, low-loss microlens arrays fabricated by soft-lithography replication process. *Appl. Phys. Lett.* **2003**, *82* (8), 1152−1154.
(45) Rogers, J. A.; Someya, T.; Huang, Y. Materials and Mechanics for Stretchable Electronics. *Science (Washington, DC, U. S.)* **2010**, *327* (5973), 1603−1607.
(46) Xu, S.; Yan, Z.; Jang, K.-I.; Huang, W.; Fu, H.; Kim, J.; Wei, Z.; Flavin, M.; McCracken, J.; Wang, R.; Badea, A.; Liu, Y.; Xiao, D.; Zhou, G.; Lee, J.; Chung, H. U.; Cheng, H.; Ren, W.; Banks, A.; Li, X.; Paik, U.; Nuzzo, R. G.; Huang, Y.; Zhang, Y.; Rogers, J. A. Assembly of micro/nanomaterials into complex, three-dimensional architectures by compressive buckling. *Science (Washington, DC, U. S.)* **2015**, *347* (6218), 154−159.
(47) Sun, Y.; Choi, W. M.; Huang, Y. Y.; Rogers, J. A.; Jiang, H. Controlled buckling of semiconductor nanoribbons for stretchable electronics. *Nat. Nanotechnol.* **2006**, *1*, 201.
(48) Hammock, M. L.; Chortos, A.; Tee, B. C. K.; Tok, J. B. H.; Bao, Z. 25th Anniversary Article: The Evolution of Electronic Skin (E-Skin): A Brief History, Design Considerations, and Recent Progress. *Adv. Mater.* **2013**, *25* (42), 5997−6038.
(49) Sokolov, A. N.; Tee, B. C. K.; Bettinger, C. J.; Tok, J. B. H.; Bao, Z. Chemical and Engineering Approaches To Enable Organic Field-Effect Transistors for Electronic Skin Applications. *Acc. Chem. Res.* **2012**, *45* (3), 361−371.
(50) Finne, R. M.; Klein, D. L. A Water-Amine-Complexing Agent System for Etching Silicon. *J. Electrochem. Soc.* **1967**, *114* (9), 965−970.

DOI: 10.1021/acsaelm.9b00099
ACS Appl. Electron. Mater. 2019, 1, 752−763

(51) Tse, J. R.; Engler, A. J. Preparation of hydrogel substrates with tunable mechanical properties. *Current protocols in cell biology* **2010**, *47*, 10.16.1.
(52) Pal, P.; Sato, K. A comprehensive review on convex and concave corners in silicon bulk micromachining based on anisotropic wet chemical etching. *Micro and Nano Systems Letters* **2015**, *3* (1), 6.
(53) Choi, T.-S.; Hess, D. W. Chemical Etching and Patterning of Copper, Silver, and Gold Films at Low Temperatures. *ECS J. Solid State Sci. Technol.* **2015**, *4* (1), N3084−N3093.
(54) Love, J. C.; Paul, K. E.; Whitesides, G. M. Fabrication of Nanometer-Scale Features by Controlled Isotropic Wet Chemical Etching. *Adv. Mater.* **2001**, *13* (8), 604−607.
(55) Cui, A.; Liu, Z.; Dong, H.; Wang, Y.; Zhen, Y.; Li, W.; Li, J.; Gu, C.; Hu, W. Single Grain Boundary Break Junction for Suspended Nanogap Electrodes with Gapwidth Down to 1−2 nm by Focused Ion Beam Milling. *Adv. Mater.* **2015**, *27* (19), 3002−3006.
(56) Saubestre, E. B. Copper Etching in Ferric Chloride. *Ind. Eng. Chem.* **1959**, *51* (3), 288−290.
(57) Bryce, C.; Berk, D. Kinetics of the dissolution of copper in iron(III) chloride solutions. *Ind. Eng. Chem. Res.* **1995**, *34* (4), 1412−1418.
(58) Burrows, W. H.; Lewis, C. T.; Saëre, D. E.; Brooks, R. E. Kinetics of the Copper-Ferric Chloride Reaction and the Effects of Certain Inhibitors. *Ind. Eng. Chem. Process Des. Dev.* **1964**, *3* (2), 149−159.
(59) Rajasekaran, P. R.; Zhou, C.; Dasari, M.; Voss, K.-O.; Trautmann, C.; Kohli, P. Polymeric lithography editor: Editing lithographic errors with nanoporous polymeric probes. *Science Advances* **2017**, *3* (6), No. e1602071.
(60) Rozhok, S.; Piner, R.; Mirkin, C. A. Dip-Pen Nanolithography: What Controls Ink Transport? *J. Phys. Chem. B* **2003**, *107* (3), 751−757.
(61) Chirvase, D.; Chiguvare, Z.; Knipper, M.; Parisi, J.; Dyakonov, V.; Hummelen, J. C. Temperature dependent characteristics of poly(3 hexylthiophene)-fullerene based heterojunction organic solar cells. *J. Appl. Phys.* **2003**, *93* (6), 3376−3383.
(62) Kautsky, H. Quenching of luminescence by oxygen. *Trans. Faraday Soc.* **1939**, *35* (0), 216−219.
(63) Hintz, H.; Egelhaaf, H. J.; Lüer, L.; Hauch, J.; Peisert, H.; Chassé, T. Photodegradation of P3HT−A Systematic Study of Environmental Factors. *Chem. Mater.* **2011**, *23* (2), 145−154.
(64) Reese, M. O.; Nardes, A. M.; Rupert, B. L.; Larsen, R. E.; Olson, D. C.; Lloyd, M. T.; Shaheen, S. E.; Ginley, D. S.; Rumbles, G.; Kopidakis, N. Photoinduced Degradation of Polymer and Polymer−Fullerene Active Layers: Experiment and Theory. *Adv. Funct. Mater.* **2010**, *20* (20), 3476−3483.
(65) Dasari, M.; Rajasekaran, P. R.; Iyer, R.; Kohli, P. Calligraphic solar cells: acknowledging paper and pencil. *J. Mater. Res.* **2016**, *31* (17), 2578−2589.
(66) van den Meerakker, J. E. A. M.; Baarslag, P. C.; Scholten, M. On the Mechanism of ITO Etching in Halogen Acids: The Influence of Oxidizing Agents. *J. Electrochem. Soc.* **1995**, *142* (7), 2321−2325.
(67) Son, D.; Kang, J.; Vardoulis, O.; Kim, Y.; Matsuhisa, N.; Oh, J. Y.; To, J. W. F.; Mun, J.; Katsumata, T.; Liu, Y.; McGuire, A. F.; Krason, M.; Molina-Lopez, F.; Ham, J.; Kraft, U.; Lee, Y.; Yun, Y.; Tok, J. B. H.; Bao, Z. An integrated self-healable electronic skin system fabricated via dynamic reconstruction of a nanostructured conducting network. *Nat. Nanotechnol.* **2018**, *13* (11), 1057−1065.
(68) Jang, J.-W.; Maspoch, D.; Fujigaya, T.; Mirkin, C. A. A "Molecular Eraser" for Dip-Pen Nanolithography. *Small* **2007**, *3* (4), 600−605.

DOI: 10.1021/acsaelm.9b00099
ACS Appl. Electron. Mater. 2019, 1, 752−763